ECSE536 Final Project Report: Analysis of Transformer-based series-resonance CMOS VCO

Laurent Viel (261181958), Mathieu Godbout (261119081),
Daniel Roulin (261296018), Hossen Alyazgi (261313569)

***Abstract*—This project studies a transformer-based series-resonance CMOS VCO presented by Zhang et al. The architecture is theoretically explicated then deconstructed through simulation in ADS from the passive tank level up to single-cell, oscillator, and multicore behavior. The passive tank analysis identifies the coupled resonant modes of the transformer network and shows how magnetic coupling separates the desired and parasitic peaks. The active single-cell simulations then quantify how device loading, coupling factor, and passive-value selection affect gain, phase, mode selectivity, and input impedance. These observations are used to guide the attempt to demonstrate sustained oscillation near the target X-band region and to evaluate whether a multicore extension can improve phase-noise behavior without excessive penalty. The overall study shows that successful series-resonance design is not obtained by moving resonances blindly with passive values alone; mode control, current delivery, parasitic sensitivity, and loading must be balanced together.**

***Index Terms*—series-resonance oscillator, transformer-based tank, CMOS VCO, phase noise, ADS, quadrature oscillator**

I. Introduction

Voltage-controlled oscillators (VCOs) are fundamental building blocks in RF and mixed-signal systems because they generate the tunable periodic signals required for frequency synthesis, clock generation, and phase-locked loops. In CMOS technologies, the most common VCO implementation is based on an LC parallel tank, mainly because it is relatively simple and well established. However, this conventional topology suffers from a fundamental tradeoff between phase-noise performance and power consumption [1], which becomes increasingly restrictive in high-frequency and low-jitter applications.

To alleviate this limitation, series-resonance (SR) oscillators have been investigated as an alternative for ultra-low-phase-noise operation [2], [3]. The interest in this approach can be understood directly from the way inductor losses are modeled. Indeed, the loss of an inductor may be represented either by a small series resistance R_s or, equivalently, by a much larger parallel resistance R_p. At resonance, the inductor and capacitor combine to form either an open circuit in a parallel configuration, with its impedance approximated by R_p, or a short circuit in a series configuration, with its impedance approximated by R_s. Because $R_s \ll R_p$, a series tank will exhibit a larger AC circulating current than a parallel tank for the same tank voltage swing. This behavior is especially attractive for oscillator design because larger passive voltage swings reduce phase-noise conversion and can therefore improve noise performance, although this comes at the cost of higher power consumption due to the larger currents.

Despite these advantages, practical implementations of SR oscillators have traditionally remained more complex than their parallel-tank counterparts. Challenges such as oscillation startup, frequency tuning, device reliability under large internal signal swings, parasitic-mode suppression, and layout complexity make the topology less straightforward to implement in CMOS [4], [5]. The paper studied in this project [8] addresses these issues by proposing a transformer-based SR CMOS VCO that makes the topology more practical while preserving its low-phase-noise potential. In the proposed architecture, the transformer is used not only as part of the resonant network, but also as a means to control impedance, manage voltage swing, and facilitate reliable frequency tuning. Furthermore, each SR cell introduces a 90° phase shift, so four identical cells are cascaded to satisfy Barkhausen's phase condition of 360°. As a result, this transformer-based four-cell architecture appears as an interesting alternative to conventional parallel-tank VCOs for low-phase-noise RF design.

II. Transformer Based versus Series Resonance

To overcome the limitations of traditional parallel-tank voltage-controlled oscillators and single-port inductor-based series oscillators, a transformer-based (two-port) series-resonance tank can be utilized [6], [7]. The primary advantage of this architecture, as seen in Fig. 1, is its ability to operate with two coupled LC tanks, which allows for higher passive voltage swings and DC isolation. Consequently, this structure yields a substantial reduction in phase noise, albeit at the expense of higher power consumption due to the larger AC currents at resonance. The passive network models the transformer with a primary inductance L_1 and a secondary inductance L_2, alongside their respective series loss resistances R_1 and R_2. These are coupled with series tuning capacitances C_1 and C_2, as well as an input equivalent capacitance C_3 that accounts for blocking and parasitic device capacitances. Because of the magnetic coupling factor k between the primary and secondary coils, the transfer function (V_{OUT}/V_{IN}) inherently exhibits two distinct resonant peak frequencies.

These dual peak frequencies, denoted as ω_{x1} and ω_{x2}, represent the in-phase and out-of-phase current modes of the tank, respectively. The analytical expression for these resonant frequencies is mathematically defined as:

$$\omega_{x1,2} = \sqrt{\frac{\omega_1^2 + \omega_2^2 \pm \sqrt{\omega_1^4 + (4k^2 - 2)\omega_1^2\omega_2^2 + \omega_2^4}}{2(1 - k^2)}}. \quad (1)$$

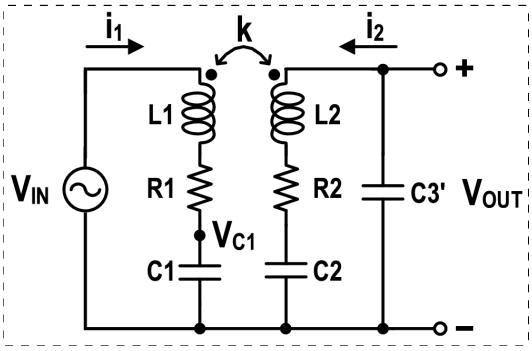

Fig. 1. Equivalent circuit model of the two-port transformer-based series-resonance passive tank.

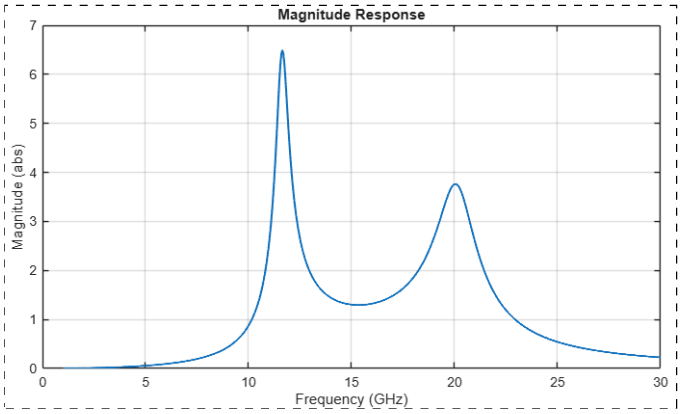

Fig. 2. Theoretical frequency response of the tank.

where ω_1 and ω_2 are the independent resonant frequencies of the primary and secondary tanks. For optimal oscillator design, it is critical that the circuit oscillates at the primary peak ω_{x1}, which provides a higher voltage gain and the necessary 90° leading phase shift, while effectively suppressing the parasitic mode at ω_{x2}. Theoretical MATLAB evaluations of this magnitude and phase response, as shown in Fig. 2 confirm the expected behavior of the transformer network. Using design parameters of L_1=250 pH, L_2=500 pH, and C_1=C_2=C_3=0.5 pF, along with quality factors Q_1=Q_2=15 and a coupling coefficient k=0.5, the series resistances are calculated to be R_1=1.491 Ω and R_2=2.981 Ω.

Plotting the theoretical magnitude response using these exact parameters reveals a dominant primary resonant frequency (F_1) at 11.623 GHz and a weaker secondary peak (F_2) at 20.132 GHz. Furthermore, analyzing the transfer function highlights that increasing the magnetic coupling factor k effectively separates the two resonant peaks, pushing ω_{x2} further into the high-frequency stopband and attenuating its magnitude. This structural characteristic is essential for ensuring that Barkhausen's criteria is satisfied exclusively at the fundamental frequency, thereby preventing unwanted mode ambiguity and ensuring reliable, low-phase-noise operation.

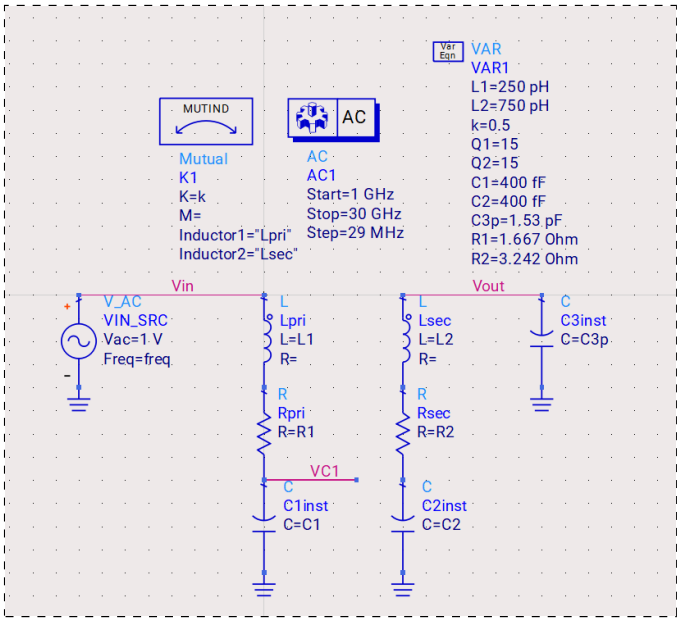

Fig. 3. Passive transformer-based tank schematic in ADS.

III. Single Cell

We begin with the passive transformer-based tank, shown in Fig. 3, because it reveals the resonant structure that the active devices must eventually sustain. For the nominal passive tank, the values are L_1 = 250 pH, L_2 = 500 pH, k = 0.5, Q_1 = Q_2 = 15, C_1 = 500 fF, C_2 = 500 fF, and C_3' = 500 fF. Under these conditions, the isolated tank sections are chosen so that w1 and w2 are approximately aligned before coupling is applied.

The ADS response in Fig. 4 then shows the effect of coupling directly: the single uncoupled resonance condition splits into two observable peaks. The lower coupled peak occurs at 11.64 GHz with $|Vout/Vin|$ = 6.48, while the higher parasitic peak occurs at 20.05 GHz with $|Vout/Vin|$ = 3.76. At the intermediate node VC1, the corresponding peaks are $|VC1/Vin|$ = 9.33 at 11.59 GHz and $|VC1/Vin|$ = 5.32 at 20.14 GHz. The peak ratio in Vout is therefore about 1.72, which confirms that the lower mode is naturally favored over the higher one.

The active single-cell, whose schematic is shown in Fig. 5, shows how this modal picture changes once transistor loading is introduced. For the nominal case in Fig. 6, the dominant gain peak is $|Vout/Vinp|$ = 1.42 at 11.70 GHz and the secondary peak is 0.87 at 20.05 GHz. The two coupled modes are still visible, but their amplitudes are reduced because the active devices and bias network load the tank.

Increasing the coupling factor from k = 0.5 to k = 0.7 strengthens the magnetic interaction and spreads the two modes farther apart. In Fig. 7, the dominant peak shifts to 10.98 GHz with magnitude 1.50, while the parasitic peak moves out to 26.00 GHz and falls to 0.71. This is the practical meaning of larger k: the desired and parasitic modes become less ambiguous, so it becomes easier for the cell to favor w_{x1} over w_{x2} . A second way to improve separation is shown in

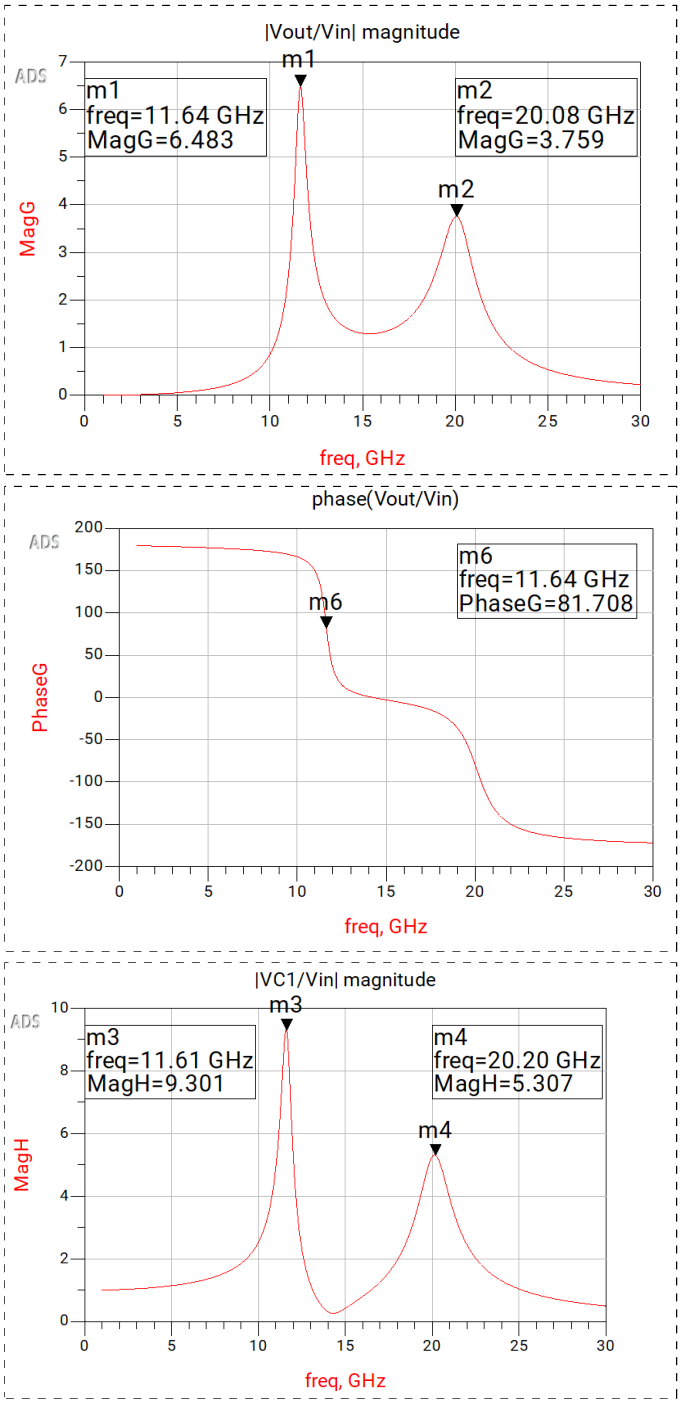

Fig. 4. Passive tank ADS responses.

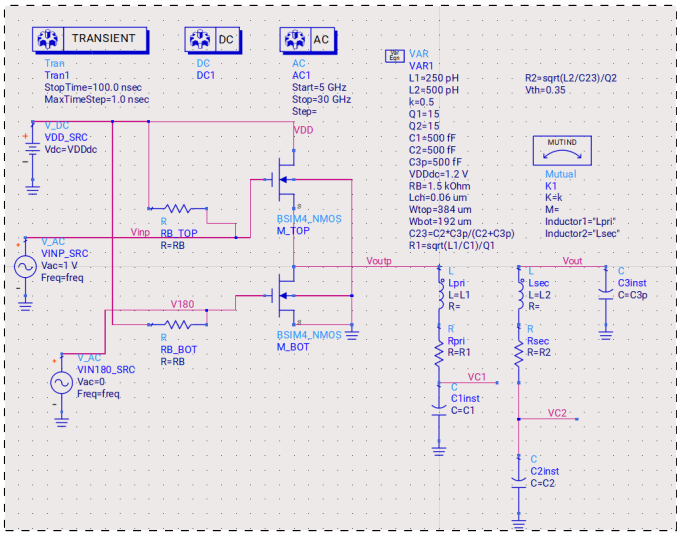

Fig. 5. Active single-cell schematic.

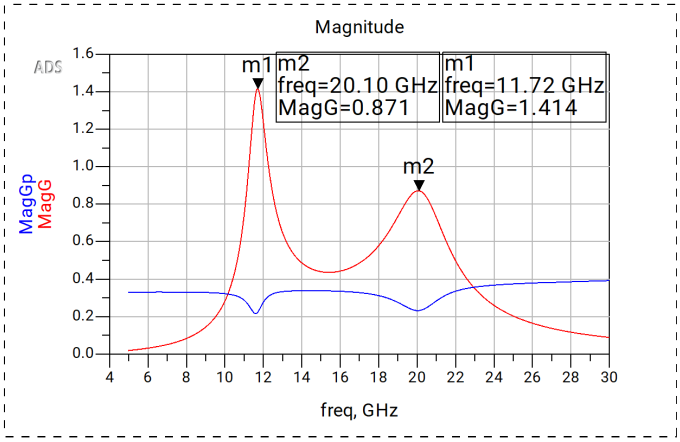

Fig. 6. Nominal active single-cell response.

Fig. 8, where L_2 is increased to 750 pH and the capacitors are reduced to C_1 = 300 fF and $C_2 = C_3'$ = 450 fF. In that case, the dominant peak is 1.15 at 11.43 GHz and the parasitic peak drops to 0.55 at 22.83 GHz. Both approaches suppress the unwanted mode, but they do not do so in equally desirable ways.Retuning the actual capacitors and inductors to push the parasitic peak away is not ideal when taken too far. First, smaller physical capacitors are more vulnerable to layout and device parasitics, so the intended resonance becomes increasingly sensitive to interconnect capacitance, transistor capacitance, and modeling error. This makes the operating point less robust and reduces confidence that the simulated frequency placement will survive a more realistic implementation. Second, increasing the effective ratio between the two tank resonances raises the input impedance of the network. A higher input impedance means less current can be driven through the resonant path. That works against the central advantage of series-resonance design, which is to support strong circulating current and large passive voltage swing.

IV. Transformer Based VCO

Building up from the single cell design, a transformer based voltage-controlled oscillator can be designed by chaining four cells in series to achieve a 360° phase shift, as proposed by Zhang et al. [8], as shown in Fig. 9.

By using a noise controller, shown in Fig. 10, phase noise spectrum can be measured around the carrier frequency in 1Hz

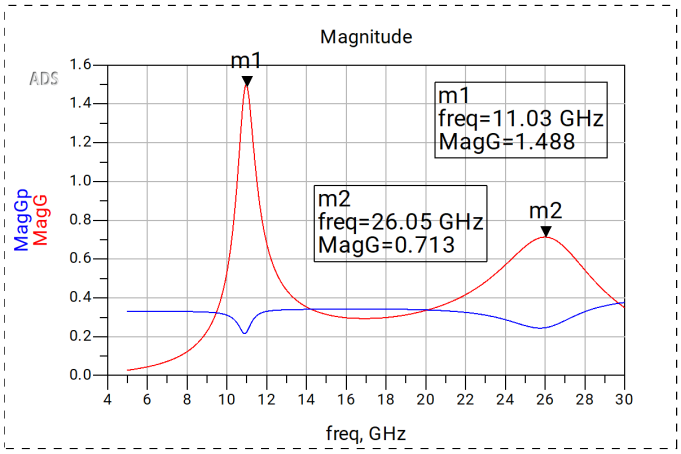

Fig. 7. Active single-cell response with increased coupling factor.

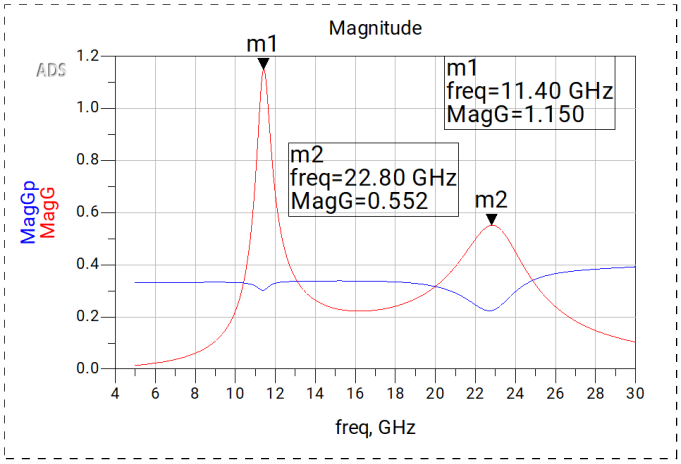

Fig. 8. Active single-cell response with modified passive values.

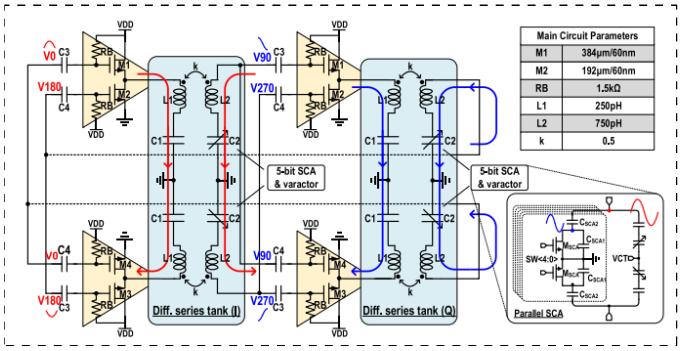

Fig. 9. Transformer based voltage-controlled oscillator architecture.

bandwidths. A current probe is also used to measure power consumption, and the harmonic balance controller can sweep to find the oscillation frequency and voltage.

As we can see in Fig. 11, the system sustains oscillation at 11.28 GHz, and has a peak to peak voltage of 7.441V for a power consumption of 638mW.

Also, the predicted phase noise curve in Fig. 12 by Zhang et al. [8] appears, showcasing the second peak due to inductor coupling:

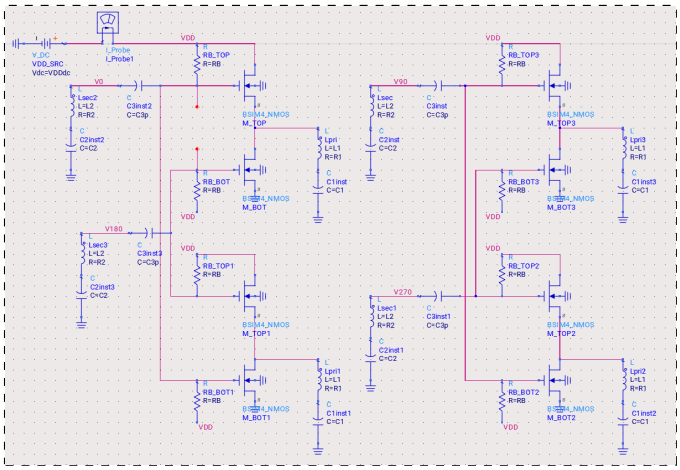

Fig. 10. ADS setup used for oscillator and phase-noise simulation.

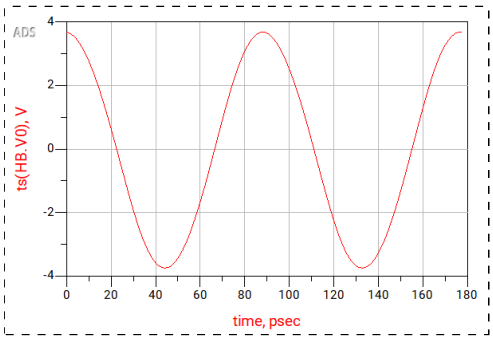

freq	P	fosc	vosc
0.0000 Hz	0.638	11.28 GHz	7.441 V

Fig. 11. Oscillation waveform and operating summary.

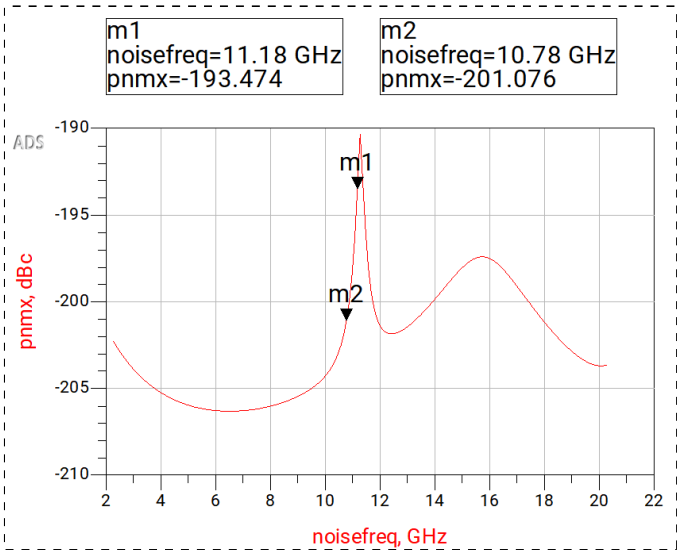

Fig. 12. Predicted phase-noise curve for the transformer based VCO.

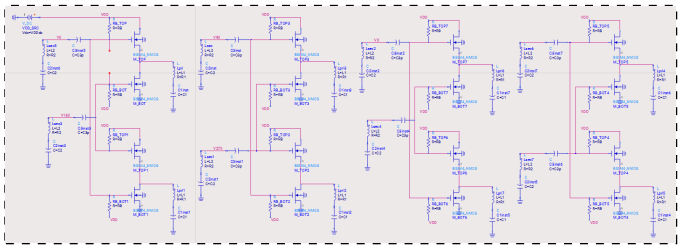

freq	P	fosc	vosc
0.0000 Hz	1.276	11.28 GHz	7.441 V

Fig. 13. Dual-core transformer based voltage-controlled oscillator design and operating summary.

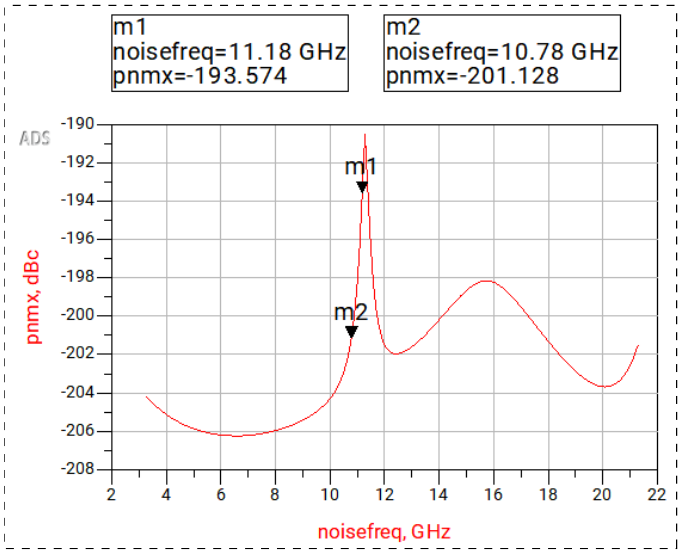

Fig. 14. Phase-noise curve for the dual-core design.

We note a phase noise of -193dBc/Hz at 100MHz from the carrier frequency, and -201dBc/Hz at 500MHz. Note that these values strongly differ from the work of Zhang et al. due to the difference between a controlled environment as ADS Keysight, and real life scenarios such as Zhang et al.'s laboratory.

V. Multi-Core Transformer Based VCO

Subsequent research by Zhang et al. [9] showcased a multi-core series-resonance design, where for the total number of cores N, the power consumption would increase but the phase noise would decrease by $10log(N)$. As an attempt to improve the design, this paper will evaluate a multi-core transformer based voltage-controlled oscillator design.

Given the above dual-core design in Fig. 13, we find the exact same oscillation frequency, voltage, and double the power consumption.

Unfortunately, the design does not showcase the expected improvement of $10log(2)$, which translates to -3dB.

In Fig. 14, we see an improvement of -0.1dB at 100MHz and -0.632dB at 500MHz from the carrier. This unfortunately showcases what is mentioned by Zhang et al. [8], where multi-core techniques can only partially improve voltage controlled oscillator designs. This yields a marginal improvement compared to the increase in power consumption.

VI. Conclusion

This project developed the transformer-based series-resonance VCO study in a layered way, beginning with passive modal behavior, then active single-cell gain and phase, then oscillator-level evaluation, and finally a multicore extension. Demonstrating sustained oscillation requires the active cell to provide enough gain at w_{x1} while avoiding conditions that allow w_{x2} to compete or that overly weaken the current through the tank. The multicore investigation also underscores the difficulties in effectively scaling the functionality of the VCO. In principle, distributing the oscillation across multiple cores can improve phase noise, but in practice the benefit is limited if the added cores introduce extra loading, power consumption, or mode-control difficulty.

References

[1] A. Hajimiri and T. H. Lee, "A general theory of phase noise in electrical oscillators," *IEEE J. Solid-State Circuits*, vol. 33, no. 2, pp. 179–194, Feb. 1998.

[2] P. Andreani, L. Fanori, and T. Mattsson, "Series-resonance oscillator," U.S. Patent 20 150 381 157, Dec. 31, 2015.

[3] F. Pepe, A. Bevilacqua, and P. Andreani, "On the remarkable performance of the series-resonance CMOS oscillator," *IEEE Trans. Circuits Syst. I, Reg. Papers*, vol. 65, no. 2, pp. 531–542, Feb. 2018.

[4] A. Franceschin, D. Riccardi, and A. Mazzanti, "Series-resonance BiCMOS VCO with phase noise of -138dBc/Hz at 1MHz offset from 10 GHz and -190 dBc/Hz FoM," in *IEEE Int. Solid-State Circuits Conf. (ISSCC) Dig. Tech. Papers*, vol. 65, France, Feb. 2022, pp. 1–3.

[5] A. Franceschin, D. Riccardi, and A. Mazzanti, "Ultra-low phase noise X-band BiCMOS VCOs leveraging the series resonance," *IEEE J. Solid-State Circuits*, vol. 57, no. 12, pp. 3514–3526, Dec. 2022.

[6] H. C. Lugon and J. Yin, *Transformer-based design techniques for oscillators and frequency dividers*, Berlin: Springer, 2015.

[7] A. Bevilacqua, F. P. Pavan, C. Sandner, A. Gerosa, and A. Neviani, "Transformer-Based Dual-Mode Voltage-Controlled Oscillators," vol. 54, no. 4, pp. 293–297, Apr. 2007.

[8] S. Zhang et al., "A Transformer-Based Series-Resonance CMOS VCO," *IEEE Journal of Solid-State Circuits*, vol. 60, no. 2, pp. 529–542, Feb. 2025.

[9] S. Zhang, W. Deng, H. Jia, Z. Wang, and B. Chi, "A Multi-Core Series-Resonance CMOS Oscillator," *IEEE Journal of Solid-State Circuits*, vol. 60, no. 5, pp. 1644–1655, May 2025.

[10] G. Li and E. Afshari, "A low-phase-noise multi-phase oscillator based on left-handed LC-ring," *IEEE J. Solid-State Circuits*, vol. 45, no. 9, pp. 1822–1833, Sep. 2010.

[11] M. Tohidian, S. A.-R. Ahmadi-Mehr, and R. B. Staszewski, "A tiny quadrature oscillator using low-Q series LC tanks," *IEEE Microw. Wireless Compon. Lett.*, vol. 25, no. 8, pp. 520–522, Aug. 2015.

[12] Y. Chen, M. Babaie, and R. B. Staszewski, "A 350-mV 2.4-GHz quadrature oscillator with nearly instantaneous start-up using series LC tanks," in *Proc. IEEE Asian Solid-State Circuits Conf. (A-SSCC)*, Nov. 2017, pp. 104–108.